ELSEVIER

Journal of Alloys and Compounds 293–295 (1999) 893–899

Journal of ALLOYS AND COMPOUNDS

Solubility and partitioning of hydrogen in metastable Zr-based alloys used in the nuclear industry

D. Khatamian*

AECL, Chalk River Laboratories, Stn. 82, Chalk River, ON K0J-1J0 Canada

Abstract

Terminal solubility and partitioning of hydrogen in Zr–Nb alloys with different niobium concentrations were examined using differential scanning calorimetry and hot vacuum extraction mass spectrometry. Specimens were charged to different concentrations of hydrogen and annealed at 1123 K to generate a two-phase structure consisting of α-Zr (Zr–0.6 wt.% Nb) and metastable β-Zr (Zr–20 wt.% Nb) within the alloy. Specimens were aged at 673 and 773 K for up to 1000 h to evaluate the effect of the decomposition of the metastable β-Zr to α-Zr+β-Nb on the solubility limit. The results show that the solubility limit for hydrogen in the annealed Zr–Nb alloys is higher than in unalloyed Zr and that the solubility limit increases with the niobium concentration of the alloy. They also show that the hydrogen solubility limits of the completely aged Zr–Nb alloys are similar and approach the values for pure α-Zr. The solubility ratio of hydrogen in β-Zr (Zr–20 wt.% Nb) to that in α-Zr (Zr–0.6 wt.% Nb) was found to range from 9 to 7 within the temperature range 520–580 K.

Keywords: Hydrogen; Solubility; Zr–Nb alloys; TSS; CANDU

1. Introduction

Due to their favorable neutronic properties, zirconium-based alloys such as the Zircaloys and Zr–Nb alloys are used for reactor core components. The effects of hydrogen on these components are of considerable interest to the nuclear industry. The components can become susceptible to a process called Delayed Hydride Cracking (DHC) when their hydrogen concentration exceeds the terminal solid solubility (TSS). Therefore, accurate values of the TSS are needed to assess the operating and end-of-life behaviour of these components. The knowledge of the variation of the TSS due to changes in the microstructure of the materials is also essential in developing new alloys with higher TSS for hydrogen without compromising other mechanical and corrosion properties.

The TSS for hydrogen in the Zr-based alloys is very low even at moderately high temperatures [1–6]. For example in Zr–2.5Nb (Zr–2.5 wt.% Nb), a two-phase alloy used for pressure tubes in CANDU® power reactors [3], the solubility limit is less than 0.7 at.% H (about 70 wt. ppm) at 573 K. Where hydrogen ingress into the alloy is a slow but continuous process (e.g. due to high temperature corrosion), higher TSS translates to longer lifetimes for the components and great savings for the industry.

The CANDU® pressure tubes are located in the core of the reactor and contain the fuel bundles and the heavy water (D_2O) heat transport fluid. The pressure tubes operate at temperatures ranging from 520 K at the inlet to 580 K at the outlet. The microstructure of the as-extruded tubes consists of elongated grains of close-packed hexagonal (cph) α-Zr (90% of volume) which contains about 0.6 wt.% Nb surrounded by a network of body-centered cubic (bcc) β-Zr (10%) which contains at least 20 wt.% niobium. The β-Zr phase is metastable at temperatures below 900 K [7] and gradually transforms via

$$(\beta\text{-Zr}) \rightarrow (\beta\text{-Zr}_{enr} + \omega) \rightarrow (\alpha + \beta\text{-Zr}_{enr} + \omega) \rightarrow (\alpha + \beta\text{-Zr}_{enr}) \rightarrow (\alpha\text{-Zr} + \beta\text{-Zr}_{enr} + \beta\text{-Nb})$$

to the constituent elements α-Zr and β-Nb [8]. Here $\beta\text{-Zr}_{enr}$ means β-Zr enriched in Nb to concentrations more than 20 wt.%. Early measurements had shown that the TSS for hydrogen in the β-Zr (Zr–20 wt.% Nb) phase is higher than in the α-Zr [9] and that the relative solubility of hydrogen in Zr–20Nb to that in zirconium is higher than unity. Later studies [10] confirmed these early findings and also showed that the relative solubility decreases with the decomposition of the β-phase. With this background it was

*Corresponding author.

0925-8388/99/$ – see front matter
PII: S0925-8388(99)00388-6

suggested that the TSS for hydrogen in Zr–2.5Nb pressure tube material must be higher than in Zr or other α-Zr phase alloys such as Zircaloy-2 and -4. Therefore, a systematic study of the TSS for hydrogen in Zr–Nb alloys with different concentrations of niobium was initiated. Thus far unalloyed Zr, Zr–1Nb, Zr–2.5Nb, Zr–5Nb, Zr–10Nb, Zr–15Nb and Zr–20Nb alloys both in the fully regenerated and the completely decomposed β-Zr variations have been investigated. In all these alloys the concentration of the constituent elements are given in wt.%. The results obtained from unalloyed Zr and the Zr–20Nb alloys were reported earlier [11]. The results from the rest of the alloys along with some preliminary results from the Zr–2.5Nb pressure tube material, with β-phase decomposed to different degrees, will be discussed here.

2. Experimental

Specimens of Zr–1Nb, Zr–5Nb, Zr–10Nb and Zr–15Nb alloys (4×30×1 mm) were cut from 1 mm-thick sheet material. Specimens of 3×3×20 mm size were machined from a piece of unirradiated Zr–2.5Nb pressure tube (No. RX078). All the alloys were obtained from Oremet Wah Chang, Albany. According to the chemical analysis, the major impurities were oxygen, iron and carbon at 1200, 460 and 110 wt. ppm, respectively. The specimens were annealed in vacuum at 1123 K for 1 h and cooled to room temperature within about 30 min to transform the alloy to the mixed phase (α-Zr+β-Zr). This heat treatment also changes the microstructure of the Zr–2.5Nb pressure tube specimens from one of highly elongated α-Zr grains into one with nearly equiaxed α-Zr grains interspersed with β-Zr phase either at triple points or along the long axis of the α-Zr grains [12].

After annealing, hydrogen was introduced to the specimens from the gas phase at 673 K to provide a range of hydrogen concentrations. Then the specimens were sealed individually in quartz tubes under vacuum and annealed at 1123 K again to homogenize the specimens with respect to hydrogen and to regenerate the β-Zr phase. Subsequent examination of the lattice parameter of the β-Zr phase of specimens by X-ray diffraction confirmed that the bcc structure with ~20 wt.% Nb was regenerated (for lattice parameter variation of the β-phase vs. Nb concentration see [13]). Some of the specimens were aged in vacuum at 773 K for 1000 h [8]. After aging, X-ray diffraction showed that they had completely transformed to (α-Zr+β-Nb) phase. Some of the Zr–2.5Nb specimens were also given two intermediate anneals at 673 K for 24 and 96 h to simulate the pressure tube stress relieving process carried out at the final stage of pressure tube fabrication.

Coupons of 3×3×2 and 4×4×1 mm size were cut from each specimen and analyzed using Differential Scanning Calorimetry (DSC) technique to obtain the hydride dissolution temperatures. A TA Instruments[1] DSC 2910 was used for the measurements. A hydrogen-free coupon of similar size, weight and the alloy composition to the specimen was used as the reference. It was obtained by heating the coupon to 1400 K in an ultra-high vacuum chamber. The hydrogen concentration of the reference coupon is less than 1 mg kg^{-1}. The resulting differential heat flow reflected the dissolution/precipitation of hydrides in the specimen.

Each specimen was analyzed for the phase transition temperature in at least three consecutive thermal cycle runs. The runs consisted of a heatup from a temperature within the range 250–300 K to some maximum temperature, T_{max}, a hold-time of 5 min at T_{max} followed by a cooldown to the same lower temperature. In all runs the heatup/cooldown rate was 30 K min^{-1}. The first run served to condition the specimens with the same thermal treatment immediately prior to any subsequent runs, since prior thermal history can affect the results. For all the aged specimens, T_{max} was chosen to be 723 K. However, in the case of the annealed specimens (containing β-Zr) the lowest possible T_{max}, was used to minimize the potential transformation of metastable β-Zr structure. The T_{max} was chosen to be at least 30 K higher than the estimated hydride dissolution temperature so that the DSC heatflow signal would include the completion of the hydride dissolution process. The instrument was regularly calibrated using melting points of indium (429.76 K), tin (505.04 K) and lead (600.65 K). Following the DSC measurements, the specimens were analyzed for hydrogen concentration by the Hot Vacuum Extraction Mass Spectrometry (HVEMS) technique [14]. It has been shown [6] that TSS in zirconium and its alloys displays a strong hysteresis and depends on whether hydrides are dissolving (TSSD) or precipitating (TSSP). The hydride dissolution temperature has a unique value, however, the hydride precipitation temperature depends on T_{max} and to a lesser degree on hold-time and cooling rate. Only TSSD results are described in this paper.

3. Results

Fig. 1 shows a typical DSC heat flow curve along with its temperature derivative. Three temperatures are marked in the figure; namely the Peak Temperature (PT), the Maximum Slope Temperature (MST) and the Completion Temperature (CT). As discussed earlier [11], the PT represents the hydride dissolution temperature, T_{TSSD}.

[1] TA Instruments Inc., 109 Lukens Drive, New Castle, DE 19720-0311, USA.

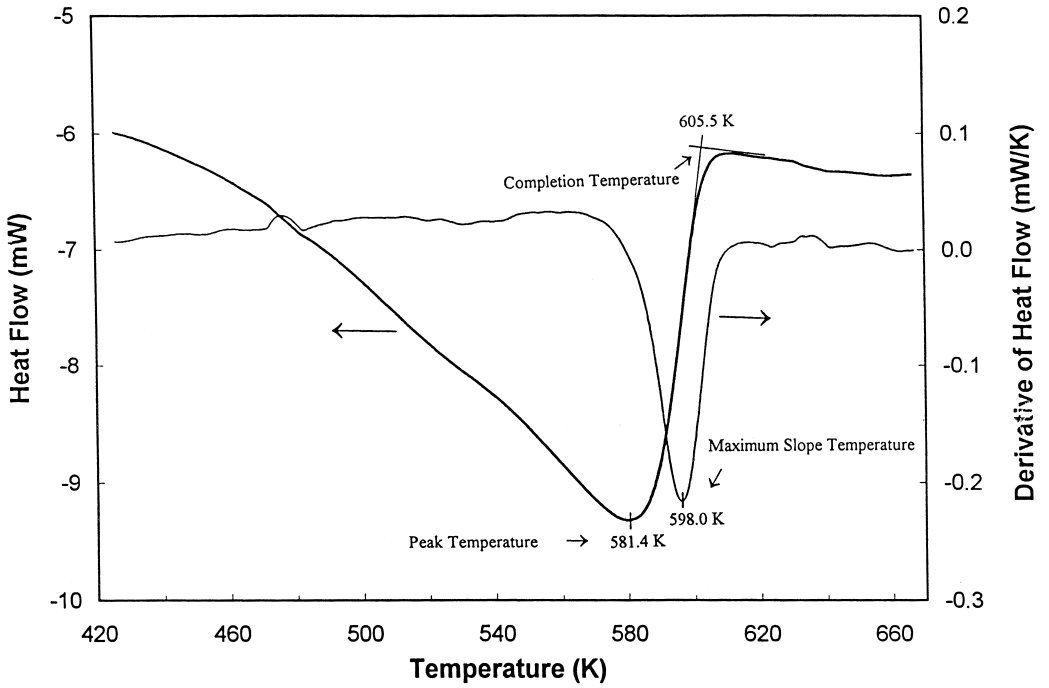

Fig. 1. DSC data from an α-Zr specimen with hydrogen concentration of 63±3 mg kg^{-1} obtained during heatup. Shown are the basic heat flow response and its temperature derivative.

Therefore, all the TSSD temperatures reported here are based on the PT.

3.1. Zr–1Nb

The hydrogen solubility limits (TSSD) in the annealed and the aged Zr–1Nb coupons were examined in the temperature range of 470–670 K. The best fit to the data, determined by linear regression of $\log C_H$, hydrogen concentration, vs. $1/T$, gives the relationships:

$$C_H = 1.83 \times 10^5 \exp(-3.71 \times 10^4/RT) \quad \text{for annealed Zr–1Nb} \tag{1}$$

$$C_H = 1.39 \times 10^5 \exp(-3.64 \times 10^4/RT) \quad \text{for aged Zr–1Nb} \tag{2}$$

where C_H is mg of H/kg of alloy, R is the universal gas constant and the number in the exponent is given here and in the subsequent equations in J mol^{-1}. The results indicate that the hydrogen solubility limits in the aged Zr–1Nb, after complete decomposition of the β-Zr phase, are lower than the solubility limits in the annealed Zr–1Nb material.

3.2. Zr–2.5Nb

The hydrogen TSSD values for the annealed and the fully aged Zr–2.5Nb material are given in Fig. 2 along with the TSSD line, for Zr–2.5Nb alloy, measured by Slattery using dilatometry [4,5]. The solubility limits obtained from two sets of Zr–2.5Nb specimens, aged at

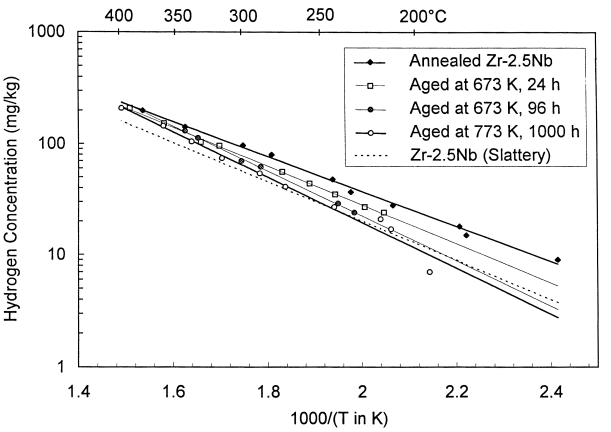

Fig. 2. TSSD for hydrogen in Zr–2.5Nb annealed at 1123 K for 1 h (solid diamonds), aged at 673 K for 24 h (open squares) and for 96 h (solid circles) and aged at 773 K for 1000 h (open circles). The solid lines are the best fits to the data. The dotted line from Slattery [4] is included for comparison.

673 K for 24 and 96 h are also plotted in Fig. 2. The measurements were carried out within the temperature range of 420–670 K. The best fit to the data gives the following equations:

$$C_H = 5.28 \times 10^4 \exp(-3.02 \times 10^4/RT) \quad \text{for annealed Zr–2.5Nb} \tag{3}$$

$$C_H = 8.85 \times 10^4 \exp(-3.35 \times 10^4/RT) \quad \text{for aged at 673 K, 24 h} \tag{4}$$

$$C_H = 2.48 \times 10^5 \exp(-3.87 \times 10^4/RT) \quad \text{for aged at 673 K, 96 h} \tag{5}$$

$$C_H = 2.41 \times 10^5 \exp(-3.92 \times 10^4/RT) \quad \text{for aged at 773 K, 1000 h} \tag{6}$$

Fig. 2 shows that the annealed Zr–2.5Nb pressure tube material, with fully regenerated β-Zr phase, has the highest TSSD and that the TSSD decreases as the β-phase decomposes. It also shows that TSSD is lowest for Zr–2.5Nb pressure tubes with fully decomposed β-phase [Eq. (6)]. These results are very close to the TSSD values for unalloyed zirconium and are similar to Slattery's line (see Section 4).

3.3. Zr–5Nb

The hydrogen solubility limits in the annealed and the aged Zr–5Nb materials were measured in the temperature ranges of 420–620 K and 490–630 K, respectively. The best fit to the data resulted in the following equations:

$$C_H = 7.38 \times 10^4 \exp(-3.01 \times 10^4/RT) \quad \text{for annealed Zr–5Nb} \tag{7}$$

$$C_H = 3.08 \times 10^5 \exp(-3.99 \times 10^4/RT) \quad \text{for aged Zr–5Nb} \tag{8}$$

The results show that the TSSD for the annealed material is much higher than that for the aged material.

3.4. Zr–10Nb

Due to the high volume fraction of the metastable β-Zr phase in annealed Zr–10Nb alloy, the TSSD measurements were made over a lower temperature range of 350–430 K to obtain acceptable DSC signals. For the aged material the temperature range was 470–670 K. Analysis of the data results in the following equations:

$$C_H = 4.66 \times 10^4 \exp(-1.99 \times 10^4/RT) \quad \text{for annealed Zr–10Nb} \tag{9}$$

$$C_H = 3.05 \times 10^5 \exp(-4.02 \times 10^4/RT) \quad \text{for aged Zr–10Nb} \tag{10}$$

3.5. Zr–15Nb

The data from the Zr–15Nb specimens showed that the annealed Zr–15Nb material is highly metastable and transforms to a large degree even during short DSC thermal cycles. Even though the temperature range of the measurements was kept to the lowest, 340–440 K, it was impossible to obtain a unique TSSD line for this alloy under present conditions. Therefore, the data points given in Fig. 3 are not very reliable and are solely presented to show the effects of the β-phase decomposition on the TSSD. Further measurements at lower hydrogen concentrations and as a consequence at lower temperatures may provide more acceptable results. Note that the alloy Zr–20Nb [11] is stable enough to obtain consistent results. The reason for the difference between the stability of Zr–15Nb and Zr–20Nb is not known.

The aged Zr–15Nb specimens were examined within the temperature range of 570–770 K. In this case the DSC results were consistent and the analysis of the data resulted in the following equation:

$$C_H = 1.76 \times 10^5 \exp(-3.9 \times 10^4/RT) \quad \text{for aged Zr–15Nb} \tag{11}$$

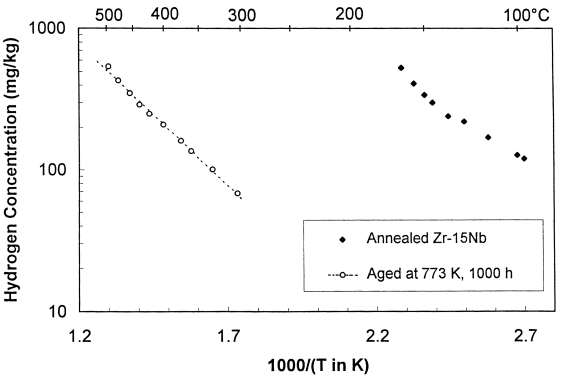

Fig. 3. TSSD for hydrogen in Zr–15Nb annealed at 1123 K for 1 h (solid diamonds) and aged at 773 K for 1000 h (open circles). The dotted line is the best fit to the data from the aged specimens. Due to inconsistency of the data from the annealed specimens (solid diamonds) no attempt was made to fit them to any model (see text).

The experimental data for aged Zr–15Nb along with Eq. (11) are plotted in Fig. 3.

4. Discussion

The dashed line in Fig. 2 is the TSSD line obtained by Slattery [4,5] for Zr–2.5Nb alloy. This line is closer to the present results for the aged specimens than for the annealed ones, but it has slightly lower slope than the present results. Generally, the agreement is good due to the fact that the specimens used by Slattery were also considerably aged during preparation. However, depending on the hydrogen concentration they were aged various degrees. The specimens, obtained from a piece of material annealed at 993 K and cold worked to about 80%, were electrolytically hydrided and annealed at 523–773 K for 100–77 h to attain different hydrogen concentrations. They were finally annealed at 753 K for 1 h to ensure homogeneity. Since higher temperatures were used to obtain specimens with higher hydrogen concentrations, the β-Zr phase decomposed to a higher degree in these specimens than in those with lower hydrogen concentrations. As a result, the level of the β-phase decomposition most likely increased with the hydrogen concentration of the specimens causing the lower slope for Slattery's TSSD line.

The equations resulting from the best fits to the data obtained from all the annealed specimens are plotted in Fig. 4. In this figure the results for unalloyed Zr (α-Zr) obtained by Khatamian and Ling [11] and Kearns [1] and for annealed Zr–20Nb (β-Zr) [11] are also presented for comparison. The figure shows that the solubility limit for hydrogen in the annealed Zr–Nb alloys is higher than in unalloyed Zr and that the solubility limit increases with the niobium concentration of the alloy. The reason for this higher solubility limit is the presence of β-Zr phase (Zr–20Nb) in these alloys and the partitioning of hydrogen between the β-Zr and the α-Zr [9,10]. (This implies that β-Zr has a higher affinity for hydrogen than α-Zr and acts as a getter of hydrogen in the Zr–Nb alloys.) It has been shown [11] that the solubility limit (TSSD) in the β-Zr phase at room temperatures is about 150 mg of H/kg of alloy. This indicates that during the entire DSC cycle, which may span from 300 to 700 K, the hydrogen in the β-phase is always in solution and that the variation in the DSC heat flow signal (Fig. 1) is solely due to the dissolution of the hydrides in the α-phase. (This of course is true only for the alloys with a small Nb concentration which have a large volume fraction of α-Zr phase.) Therefore, the TSSD temperature measured by DSC is representative of the amount of hydrogen present in the α-phase. On the other hand, the HVEMS measurements give the total amount of hydrogen in the specimen including the hydrogen partitioned to the β-Zr component. As a result, the effective solubility limit for hydrogen in the Zr–Nb alloys appear higher than the solubility limit in unalloyed Zr.

In Fig. 5 the equations resulting from the best fits to the data obtained from the aged Zr–Nb alloys are plotted. The results for Zr (α-Zr) measured by Kearns [1] and by Khatamian and Ling [11] are also included in the figure. These results show that the hydrogen solubility limits in the aged Zr–Nb alloys, due to complete decomposition of the β-Zr phase, are very close to each other and approach the values for pure Zr (α-Zr). Although the solubility limit for hydrogen in β-Nb [15] is much higher than in α-Zr, these results indicate that the solubility ratio for hydrogen in the β-Nb to that in the α-Zr must be near unity.

4.1. Partitioning of hydrogen between α-Zr and β-Zr phases in the annealed Zr–Nb alloys

The solubility ratio, ρ, for hydrogen in the β-Zr to that in the α-Zr was calculated using the TSSD data from unalloyed zirconium and the annealed Zr–Nb alloys, Zr–

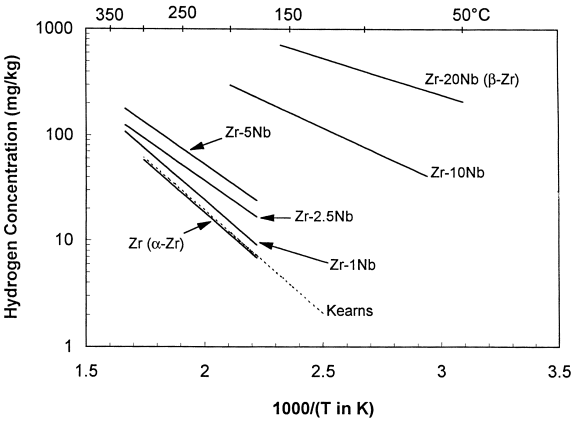

Fig. 4. TSSD lines for hydrogen in Zr–Nb specimens with different Nb concentrations annealed at 1123 K for 1 h. The lines for Zr (α-Zr) and annealed Zr–20Nb (β-Zr) [10] as well as the Kearns' line for unalloyed Zr are included for comparison.

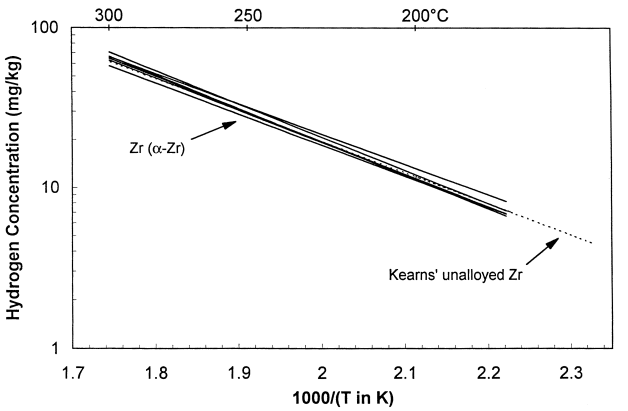

Fig. 5. TSSD lines for hydrogen in Zr–Nb specimens with different Nb concentrations aged at 773 K for 1000 h. The lines for unalloyed Zr (α-Zr) obtained by Kearns [1] and Khatamian and Ling [10] are included for comparison.

2.5Nb and Zr–5Nb. Note that the Zr–Nb alloys have the maximum β-Zr component in the annealed state. Assuming that the Nb concentrations in the α- and the β-Zr components of the alloy, in the annealed state, are C^{α}_{Nb} and C^{β}_{Nb}, respectively, the following equation can be used to determine the weight fraction of the α-Zr, w_{α}, and the β-Zr, w_{β}, phases in the annealed Zr–Nb alloys

$$(w_{\alpha}/w_{\beta}) = (C^{\beta}_{Nb} - C_{Nb})/(C_{Nb} - C^{\alpha}_{Nb})$$

where C_{Nb} is the niobium concentration of the alloy and $w_{\beta} + w_{\alpha} = 1$. The X-ray diffraction (XRD) measurements showed that C^{β}_{Nb} is about 20 wt.% [13] in the annealed Zr–2.5Nb and Zr–5Nb specimens. In addition the Zr–Nb phase diagram [7] shows that C^{α}_{Nb} is about 0.6 wt.%. We assume that the TSSD relation for hydrogen in the α-component of these alloys is similar to that for unalloyed Zr. (This is a valid assumption because the Nb concentration of this component is low.) With this assumption, the hydrogen concentration in the α-Zr phase of the alloy, $[H_{\alpha}]$, at a given temperature can be calculated using the TSSD equation for unalloyed Zr [11]. Then the following equation can be used to determine the solubility ratio, ρ.

$$\rho = ([H] - [H_{\alpha}]w_{\alpha})/([H_{\alpha}]w_{\beta})$$

where $[H]$ is the hydrogen concentration of the alloy (i.e. the total amount of hydrogen in a specimen per unit weight), determined using the TSSD equations for the annealed alloys. The calculated solubility ratios vs. temperature are plotted in Fig. 6. The small difference between the solubility ratios obtained using the TSS results from Zr–2.5Nb (solid line) and Zr–5Nb (dashed line) may not be real because they depend highly on C^{β}_{Nb} and C^{α}_{Nb} where no accurate values are available, especially in the case of C^{α}_{Nb}.

The average solubility ratios for the two alloys in Fig. 6 range from about 9 to 7 within the temperature range 520–580 K. These values are considerably higher than the solubility ratios reported by Sawatzky et al. [9] and Cann et al. [10]. Sawatzky et al. charged specimens of 1-mm thick Zr disks with hydrogen and annealed at 1073 K for 1 h in a capsule sealed together with a similar size Zr–20Nb disks. This high temperature annealing process was carried out to regenerate the β-Zr phase as well as to dissolve the surface oxide layer. They then cooled the capsule to a desired temperature and kept it there for a period long enough (ranging from 96 to 1000 h depending on the temperature) to achieve equilibrium. Afterwards, the hydrogen concentration of the specimens was determined and the relative hydrogen solubility was calculated. The maximum values they obtained were 2.59, 1.79 and 1.97 at temperatures of 523 K, 573 K and 673 K, respectively. The long heat treatments, especially at 573 K and 673 K, partially decomposed the β-Zr specimen resulting in low values for the solubility ratio. Since during equilibration two separate disks were used, it is also likely that the coupling between the two specimens was not adequate to achieve equilibrium, resulting in low solubility ratios.

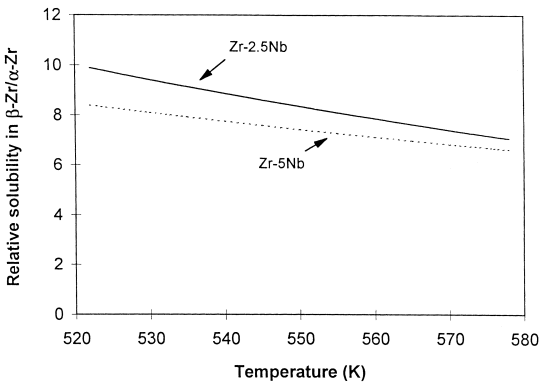

Fig. 6. The solubility ratio, ρ, for hydrogen in the β-Zr to that in the α-Zr calculated using the TSSD data from unalloyed zirconium [10] and the annealed Zr–2.5Nb [Eq. (3)] and Zr–5Nb [Eq. (7)] alloys.

Cann et al. [10] determined the effects of the β-Zr decomposition on the partitioning of hydrogen between the α- and the β-phases. Their specimens were made of welded couples (to improve the rate of transfer of hydrogen) of α-Zr and Zr–20Nb where the α-Zr component was charged with hydrogen prior to welding. The couples were then given heat treatments at 673 K for different periods to obtain specimens with different levels of β-Zr decomposition. Subsequently they were equilibrated at different temperatures and the β-phase was examined with XRD [13] for the degree of decomposition. The resulting solubility ratios ranged from 4 to 1.4 as the level of decomposition increased. They also showed that the solubility ratio increased as the equilibration temperature decreased. The specimen equilibrated at 523 K for 1200 h gave the highest solubility ratio. Although Cann et al. had exercised great care in treating their specimens and were successful to obtain higher solubility ratios than those measured by Sawatzky et al. [9], it is likely that annealing at 523 K for long periods would slightly decompose the β-phase and lower the solubility ratio to some extent.

5. Conclusions

The effects of decomposition of the metastable β-Zr (Zr–20Nb) on the solubility limit of hydrogen in Zr–Nb alloys with different Nb concentrations have been measured using differential scanning calorimetry and hot vacuum extraction mass spectrometry. Using these results the solubility ratio of hydrogen in β-Zr to that in α-Zr was also calculated. It was found that:

1. The solubility limit for hydrogen in the annealed Zr–Nb alloys, with fully regenerated β-Zr phase, is higher than in unalloyed Zr and the solubility limit increases with the total niobium concentration of the alloy.

2. The hydrogen solubility limits in the aged Zr–Nb alloys, with fully decomposed β-Zr phase, are similar and approach the values for unalloyed Zr (α-Zr).
3. The solubility ratio of hydrogen in β-Zr (Zr–20Nb) to that in α-Zr was calculated to be about 9–7 within the temperature range 520–580 K.

Acknowledgements

The skillful efforts of V.C. Ling in preparing the samples and running the DSC equipment are very much appreciated. The author wishes to thank W.A. Ferris for charging the specimens with hydrogen, J.E. Winegar for obtaining XRD patterns of some of the samples and T.G. Lamarche for analyzing the specimens for hydrogen concentration by HVEMS. Helpful discussions with A.A. Bahurmuz, C.D. Cann and M. Griffiths and critical review of the manuscript by V.F. Urbanic and C.E. Coleman are appreciated. This work was funded by AECL CANDU R&D Program 5.

References

[1] J.J. Kearns, J. Nucl. Mater. 22 (1967) 292.
[2] E. Zuzek, J.P. Abriata, A. San-Martin, F.D. Manchester, Bull. Alloy Phase Diagrams 11 (1990) 385.
[3] C.E. Ells, Met. Soc. CIM Vol. 17 (1978) 32.
[4] G.F. Slattery, J. Inst, Metals 95 (1967) 43.
[5] G.F. Slattery, J. Nucl. Mater. 32 (1968) 30.
[6] D. Khatamian, Z.L. Pan, M.P. Pulls, C.D. Cann, J. Alloys Comp. 231 (1995) 488.
[7] J.P. Abriata, J.C. Bolcich, Bull. Alloy Phase Diag. 3 (1982) 1711.
[8] B.A. Cheadle, S.A. Aldridge, J. Nucl. Mater. 47 (1973) 255.
[9] A. Sawatzky, G.A. Ledoux, R.L. Tough, C.D. Cann. In: T.N. Veziroglou (Ed.), Proc. Miami Intl. Symp. Metal–Hydrogen Systems, 13–15 April, 1981, Miami Beach, FL, pp. 109–120.
[10] C.D. Cann, E.E. Sexton, A.M. Duclos, G.G. Smith, J. Nucl. Mater. 210 (1994) 6.
[11] D. Khatamian, V.C. Ling, J. Alloys Comp. 253 (1997) 162.
[12] R.A. Holt, M. Griffiths, R.W. Gilbert, J. Nucl. Mater. 149 (1987) 51.
[13] P.E.J. Flewitt, Scripta Metall. 5 (1971) 579.
[14] L.L.W. Green, G.A. Bickel, P.K. Leeson, M.W.D. James, T.G. Lamarche, H. Michel, A hot vacuum extraction mass spectrometric system for determination of H and D in zirconium. In: L.W. Green (Ed.), Proc. 2nd Alfred O. Nier Symp. on Inorganic Mass Spectrometry, 9–12 May, 1994, Durango, CO, AECL Report No. 11342, 1996, pp. 95–99.
[15] J.F. Smith, in: T.B. Massalski, J.L. Murray, L.H. Bennett, H. Baker (Eds.), Binary Alloy Phase Diagrams, Vol. 2, ASM, Metals Park, 1986, p. 1274.